23rd International Congress on Modelling and Simulation, Canberra, ACT, Australia, 1 to 6 December 2019
mssanz.org.au/modsim2019

Investigation of plume attachment in inclined terrain profiles

R.A. Edgar [a], **J.J. Sharples** [a] **and H.S. Sidhu** [a]

[a]*Applied and Industrial Mathematics Research Group, School of Science, UNSW Canberra, Australia*

Email: j.sharples@adfa.edu.au

Abstract: Developing a comprehensive understanding of the behaviour of hot plumes associated with fires burning in steep and confined terrain is an important issue for firefighter safety. Many fatal accidents and incidents involving serious injury to firefighters (e.g. burnovers) occur on steep slopes or otherwise complex terrain. Many of these instances involve the fire escalating abruptly and unexpectedly, catching even experi-enced firefighters off guard.

Previous studies have linked these instances to dynamic modes of fire spread such as fire eruption, but the precise mechanisms driving them are still not properly understood. A number of authors have suggested a role for flame, or plume, attachment driven by the Coandă effect, which is a hydrodynamic effect that causes the flames and plume of a fire to attach to a sufficiently inclined surface. The Coandă effect has been implicated in structural firefighting disasters like the 1987 King's Cross disaster.

In the present research, we use Computational Fluid Dynamic methods to extend previous work that considered plume dynamics for fires burning in trenches within a confined tunnel. Specifically, we consider the plumes of open fires burning on slopes with various topographic profiles. Note that by 'open' we mean domains without a roof, in contrast to tunnel conditions. These open scenarios are more representative of the conditions encountered when wildland fires burn in complex terrain. We report preliminary results for fires burning in channels with 90° and 45° sidewalls.

Results from this study suggest the Coandă effect causes an otherwise rising plume, driven purely by convection, to attach to open channel surfaces for many metres ahead of fire fronts in terrains of slope above 26°. Accordingly, strong updraughts may follow channels and fan a fire's spread along eroded gullies and dry creek beds of sloping terrains and notably in directions totally divorced from that of regional winds.

Slight variations in the attachment threshold were found for different fire source energies and channel profiles which is consistent with the 26° threshold identified for rapid attachment to channel surfaces in tunnels, i.e. at the early tunnel fire phase prior to support from updraughts.

Keywords: *Plume attachment, firefighting, trench effect, CFD, fire dynamics, Coandă effect*

1 INTRODUCTION

The inclination of a surface on which a fire is burning can have a significant effect on the behaviour of the fire. The presence of a slope enhances the transfer of radiative and convective heat to combustible materials situated upslope from the fire, which results in the fire spreading more readily and more rapidly in the upslope direction. However, the exact mechanisms that drive upslope fire spread are still not well understood [Sullivan et al., 2014]. Indeed, there have been a number of instances where slope-driven fire spread has had fatal or near-fatal consequences [Drysdale, 1992; Schupfer, 2001; Viegas et al., 2009; Sharples et al., 2010]. Indeed, ensuring the safety of firefighters involved in wildland fire operations requires a deep understanding of fire behaviour. Coming to terms with the hazards of fires moving into sloping terrains is particularly important in view of their accelerated dynamics coincident with unexpectedly high winds often said to be unrelated to prevailing weather conditions [Cheney et al., 2001].

In this paper we present research that extends previous work on the dynamics of convective plumes which related to fires burning within rectangular trenches of inclined tunnels [Edgar et al., 2015, 2019]. The present research considers fire plumes emanating from triangular and rectangular channels, including ones identical to the rectangular trenches of the earlier work, however in open terrains outside of tunnels. We use Computational Fluid Dynamic (CFD) methods (implemented using the ANSYS-CFX version 19.1 software [ANSYS, 2019]) for these investigations for various terrain slopes and fire intensities. These simulations within open domains are more representative of wildland settings. Of particular interest are factors affecting plume attachment to inclined surfaces because attachment confines the fire's energy to the combustible fuel volume and therefore contributes significantly to the rapidity of a fire's spread.

2 BASELINE (BL) SIMULATION MODEL

2.1 Geometry

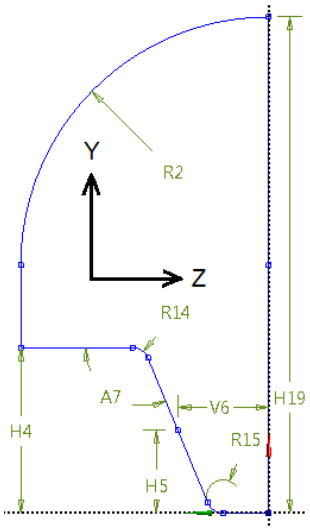

Channel	90° bank	45° bank
A7	90°	135°
H4 (m)	1.0	1.0
H5 (m)	$= 0.5 \times$ H4	$= 0.5 \times$ H4
H19 (m)	10	10
R2 (m)	4	4
R14 (m)	0.1	0.1
R15 (m)	0.1	0.1
V6 (m)	0.55	0.55

Figure 1. Not-to-scale cross-section of the vaulted numeric domain showing the mirrored left-half with its defining parameters.

The not-to-scale diagram in Figure 1 shows defining parameters of the modelled numeric domains. The baseline (BL) domain volume was created by mirroring and joining surfaces with the left cross-section shown, and then extruding the pair orthogonally 30 m.

For convenience, the definition of some terms used to reference specific surfaces or volumes of the model's geometry throughout this paper follow:

Channel - volume produced extruding area below the upper horizontal line;

Sky - volume produced extruding area above the upper horizontal line;

Ground - surfaces produced extruding the upper horizontal line;

Floor - surface produced extruding the lower horizontal line;

Lip - surfaces produced extruding the arc R14; and

Bank - surfaces produced extruding the arcs R14 and R15, and the line between them.

The origin (0, 0, 0) of the numeric domain was assigned to the point on the bottom right corner of Figure 1, i.e. middle of the trench floor at the bottom of the domain.

The slope (θ) of the terrain within which the channel sits was set by the direction of the relevant simulation's gravity vector.

The fire source volume was defined by a dedicated variable given the value one (or true) for $7\,\text{m} < x < 9\,\text{m}$ and $0\,\text{m} < y < 0.9\,\text{m}$.

2.2 Fire-energy source

The fire-energy source volume was divided channel lengthwise into eight equal sub-volume segments. The fire-energy input was switched between the source's four even and odd segments at the rate of 50Hz to allow room for local expansion of air with adjustment at a time scale compatible (but not resonant) with the BL model's 30 ms discrete timesteps.

2.3 Mesh

An unstructured mesh was generated using the ANSYS meshing module for CFX. In this research, the simulations relating to each channel cross-section all use the same mesh in order to eliminate the computational demands of re-meshing and unnecessary variations amongst the simulations.

An enlarged cross-section of the 90° bank channel is shown in Figure 2. Mesh statistics of 45° and 90° bank channel domains are listed in Table 1.

Modelling similar thermal sources in tunnel trenches of equivalent size, an equivalent mesh to that used in this study was shown to be optimal for such investigations of plume dynamics [Edgar et al., 2019]. The relevant mesh sizes of this open channel study and the similar tunnel study are listed in Table 2.

Table 1. Mesh node and element counts of the Baseline (BL) channel models.

Model	45° bank	90° bank
Nodes	7 363 572	7 399 460
Elements	19 162 452	19 074 803
– tetrahedrons	7 248 088	7 010 355
– prisms	11 914 364	12 064 448

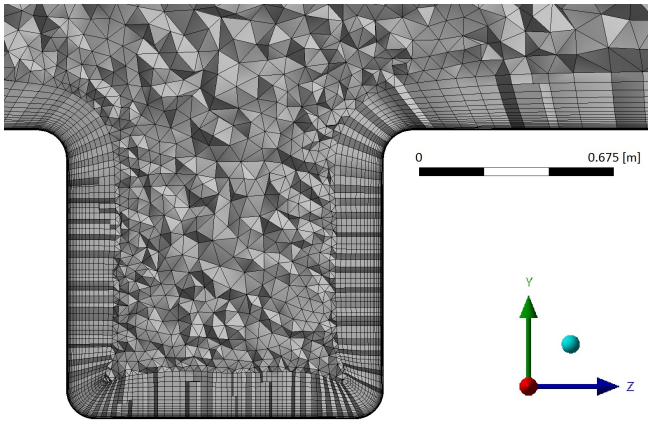

Figure 2. Detail of a cross section through the channel bank 90° domain showing trench mesh scales and thicker inflation layers over ground and trench surfaces.

Table 2. Mesh length scales used in Baseline (BL) and length scale validation models

Model	Tunnel trenches	Open channels
Counts		
- Inflation layers	22	22
Growth rates		
- Global	1.85	1.2
- Trench	1.05	1.1
Max. lengths (mm)		
- Global tet	200	200
- Global face	100	100
- Source	120	-
- Ground	-	100
- - Infl. 1st height	0.75	0.75
- Lip	-	30
- Trench	-	20

2.4 Fluid dynamic and state equations

The ANSYS© Baseline variant of the Reynolds Stress Model (RSM-BL) was chosen to simulate turbulence. The model has individual transport equations for each of the six independent components of the Reynolds stress tensor, one for turbulence energy and another blended from turbulence dissipation and turbulence

frequency representations of the flow field depending on wall distance. An exact turbulence production term and representation of stress anisotropies make the model theoretically superior to engineering standard two-equation turbulence models and better suited to simulate complex flows exhibiting strong convection and turbulence as required. The RSM-BL model blends turbulence energy dissipation (k-ϵ) with turbulence energy frequency (k-ω) representations of the flow field equations on the basis of the wall distance to overcome individual limitations of each, i.e. the former cannot be integrated all the way to the wall while the latter is overly dependent on the calibration values in the free stream far from walls [ANSYS, 2019].

Radiation from the hot plume, which would add to wall heating and increase thermal dissipation, is not included in this study however its potential effects are considered secondary due to the overwhelming influence of strong buoyancy driven mixing. A back of the envelope estimate of the plume's radiation suggests it represents less than 1% of the source's power.

Air is modelled as an ideal gas with the properties listed in Table 3.

Table 3. Properties of air modelled as an ideal gas in channel simulations.

dynamic viscosity (μ)	$1.831 \times 10^{-5}\,\mathrm{kg\,m^{-1}s^{-1}}$
molar mass (m_{mol})	$28.96\,\mathrm{kg\,kmol^{-1}}$
specific heat capacity at constant pressure ($\mathrm{c_p}$)	$1.0044 \times 10^{3}\,\mathrm{J\,kg^{-1}K^{-1}}$
adiabatic lapse rate (Γ)	$-0.0341577\,\mathrm{K\,m^{-1}}$
thermal conductivity (λ_{T})	$2.61 \times 10^{-2}\,\mathrm{Wm^{-1}K^{-1}}$

2.5 Boundary conditions and initialisation

At the reference position (0, 0, 0), i.e. centre of the channel floor at the bottom of the domain, the reference atmospheric settings were absolute pressure $P_{\mathrm{ref}} = 1$ atm, and temperature $T_{\mathrm{ref}} = 25\,\mathrm{C}$.

All above ground surfaces and the channel ends were defined as openings that allowed flow to travel in or out of the domain. Openings were given isostatic pressure and temperature gradients based on their height, i.e. derived from the simulations' defined gravity vector direction. Flows out from the model domain minimised momentum gradients while those inward were constrained to initially take a normal-to-surface direction. Other domain boundaries represent physical surfaces and were defined as adiabatic, aerodynamically smooth, non slip walls. A non-slip wall is one that imposes a surface tangential flow velocity of zero as observed in nature.

The initialisation temperature $T(x, y, z)$ at domain location (x, y, z), and the temperature of subsequent flows into the domain through openings, were defined as a function of the reference temperature and the adiabatic lapse rate, i.e.

$$T_{(x,y,z)} = T_{\mathrm{ref}} - \Gamma\,[x\,\sin(\theta) + y\,\cos(\theta)] \tag{1}$$

where $\theta =$ channel (and terrain) slope.

3 METHOD

This study considered 93 kW, 431 kW and 2000 kW channel fires in open terrains of 20–35° slope. The simulations started at $t = 0$ s with no wind present and so all flows that emerged were fully convection driven by the fire source's presence. The energy level of fire sources ramped up from zero during the first simulation second. The simulation end time was typically 50 s however occasionally longer at lower energies and slopes which took longer to mature, i.e. reach the stage when broad turbulence patterns repeat with only secondary differences.

The CFX-solver uses linear methods to solve the mass and momentum conservation equations concurrently. It then solves individual systems for energy, Reynolds stress components and turbulence dependent dissipation and frequency relations; however, an additional adjustment of the pressure distribution for the conserved mass was specifically added to iterations within timesteps to improve their response to the large thermal impulses considered.

The simulation flow field files were processed using ANSYS CFD-Post to define and export variables and with MATLAB for graphics.

The enthalpy ratio of air in the upper reach of the channel relative to that outside the channel was chosen to quantify the degree of attachment associated with hot plumes because (i) enthalpy is a fundamental property directly affecting fire propagation rates and (ii) the plumes were generally seen to detach and reattach further along the channel making the simpler distance measurements used in earlier research relating to tunnels untenable.

Discrete volume elements were considered part of the plume when they had a specific enthalpy per unit mass above 4.5 kJ kg^{-1} (or approximately 29°C), 10 kJ kg^{-1} (or approximately 35°C) and 70 kJ kg^{-1} (or approximately 100°C) for simulation fire source energies of 93 kW, 431 kW and 2000 kW respectively.

Discrete elements of the plume were considered part of the attached volume when they were in the upper reach of the channel (below the channel height) and beyond any vertical extension of the source's volume.

4 Results and Discussion

Typical channel plume volumes and temperatures from simulations at the discrete fire-source energies investigated are shown in Figure 3. The plume enthalpy cutoffs were determined qualitatively with the aim of obtaining comparable plume volume sizes despite the following challenges:

- if too high the enthalpy ratios became overly sensitive to the definition of geometric boundaries between attached and unattached volumes;
- if too low the variation of enthalpy ratios was reduced by (i) the expansion of unattached plume volume (otherwise mitigated by setting the zero reference enthalpy equal to the cutoff setting) or (ii) neglecting plume enthalpy that exited through domain open boundaries; and
- volumes inevitably varied since the degree of plume attachment affected the plume's path, time and consequently extent of the plume heading towards domain boundaries.

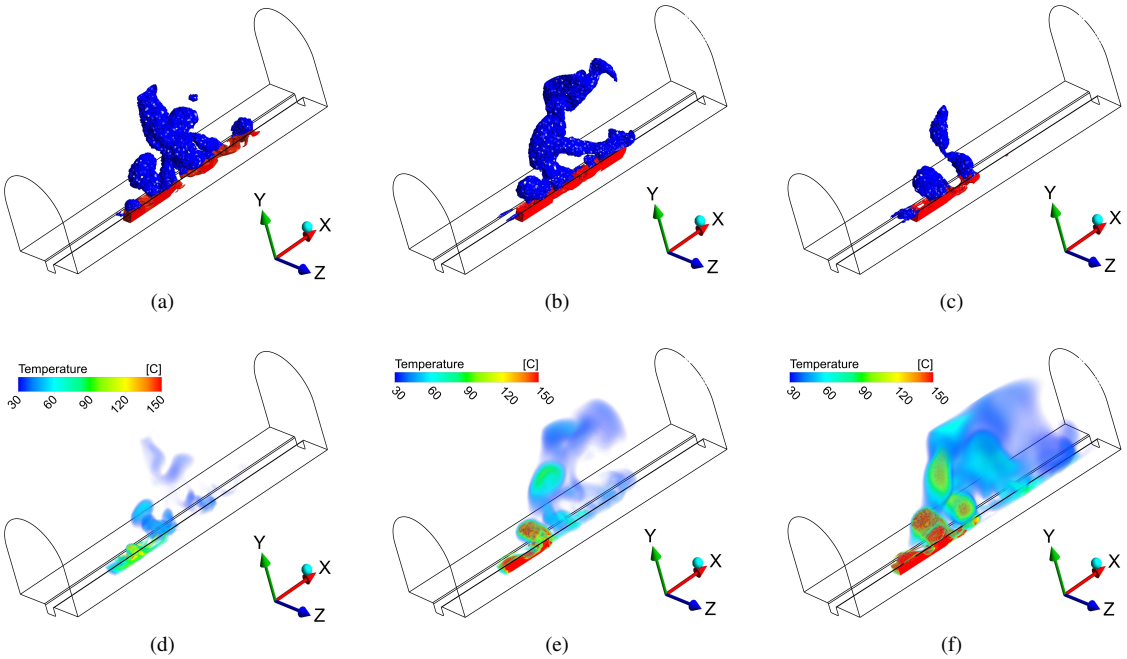

Figure 3. Simulated plume volumes for various channel configurations and fire source energies. In panels (a) to (c) the plumes are coloured red or blue when attached or unattached to channel surfaces respectively. Specifically, (a) shows the 93 kW heat source in a BL 90° bank channel inclined at 25° and simulation time 75 s, (b) shows the 431 kW heat source in a BL 90° bank channel inclined at 26° and simulation time 68 s, and (c) shows the 2000 kW heat source in a BL 90° bank channel inclined at 30° and simulation time 47 s. The concurrent temperature of domain volumes are shown below the plumes in panels (d) to (f).

The enthalpy ratio of attached to unattached plume contents obtained in BL 90° and 45° bank channel simulations are presented in Figures 4a and 4b respectively. The enthalpy ratios were found to:

- initially increase but eventually plateau for channel angles above a plume attachment threshold;

- have fairly consistent plateaus associated with each discrete source energy (excluding outlier of 93 kW source in 30° sloping channel at 38 s) and tapered off sharply 1–2 degrees above the attachment threshold;
- have threshold attachment angles that fell 1–2 degrees as source energies decreased across the twenty-fold range simulated; and
- have 1–2 degree lower attachment thresholds in the 45° bank channels.

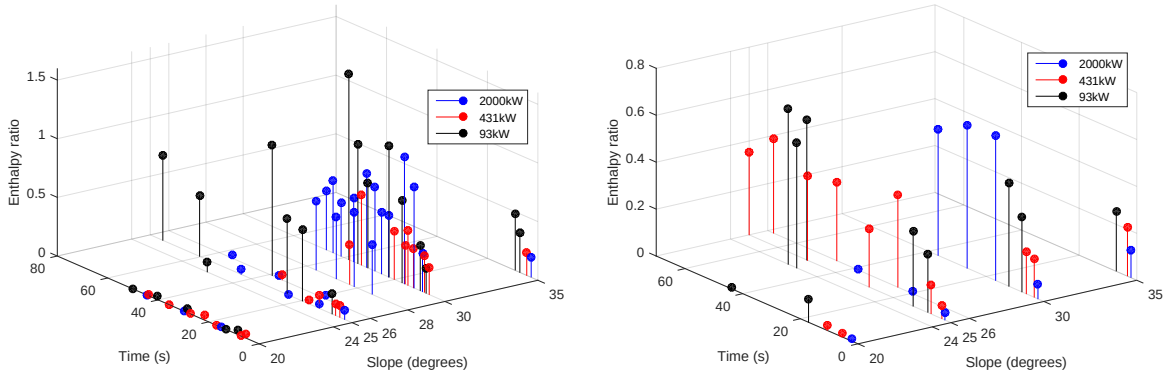

(a) The enthalpy ratio of attached to unattached plumes in channels with 90° banks is shown. Plume attachment takes longer but develops stronger (ratio >1) for the 93 kW source and occurs in terrains of slope $\theta \geq 25°$, however $\theta \geq 28°$ is needed for the plumes of 431 kW and 2000 kW sources to attach and once developed they appear to plateau at similar ratios between half and one.

(b) The enthalpy ratio of attached to unattached plumes in channels with 45° banks is shown. The terrain slope required for plume attachment appears to increases with source energy from $20° < \theta < 24°$ to $26° < \theta < 28°$ for the 93 kW and 2000 kW sources respectively. Attachment develops linearly during the first 20 s.

Figure 4. Open channel simulation plume enthalpy ratios, i.e. total static enthalpy of the plume inside versus outside the channel volume. The plume attachment in channels with 45° sides extends to a degree or two lower slopes, however otherwise appears to plateau at levels about half that found for channels with 90° sides.

The BL 90° bank channel results confirm the presence of the plume attachment threshold in the vicinity of 25–26 degrees. That corresponds with the threshold found for rapid attachment to similar trenches in tunnels, and supports the observation that plume attachment at lower tunnel slopes is impeded until sufficient convection driven updraughts develop.

Also posited from earlier tunnel trench research was a thermodynamic mechanism for Coandă like plume attachment based on the reduced momentum loss of buoyant fluids exploiting laminar surface layer conditions of sufficiently sloping trenches to climb, rather than pushing turbulent free stream paths through open air to rise [Edgar et al., 2019].

A corollary of the above plume attachment mechanism is that channels offering the most sufficiently-steep surface relative to cross-sectional area will have the lowest attachment threshold slope.

The 45° bank model has channel bank surfaces that almost meet and offers high composite-slope paths for plume attachment at threshold levels relative to that of the wide floor present in the BL 90° bank model. That is the reason suggested for the former's 1–2° lower attachment threshold. On the other hand its surface to cross-sectional area ratio is below that of the BL 90° bank model, and peak enthalpy ratios at slopes above plume attachment thresholds are generally lower accordingly.

Investigating further the change of plume attachment threshold as channel surface to cross-sectional area varies, simulations of a $\Delta xyz = 2 \times 0.9 \times 1.1\,\mathrm{m}^3$ fire source on flat terrains, and in a half width double energy-density but otherwise similar to BL 90° bank model was considered. Plume attached to unattached enthalpy ratios obtained for these topologies are shown in Figure 5.

Figure 5a shows plume attachment to flat terrains tapers but persists down to the 26° gradient level. Because channels have bank surfaces of higher composite slope than flat terrains, these results suggest the upper limit of thresholds for plume attachment to sloping channels considered collectively should similarly approach 26°.

Figure 5b shows significant plume attachment to the channel surfaces continues at slopes below 24° for the 90° bank half BL channel width model. The expanse of the channel floor between vertical banks is much reduced in this model relative to that of the BL 90° bank model, and the plume attachment threshold has been reduced at least 1–2° despite its source's doubled fire energy density.

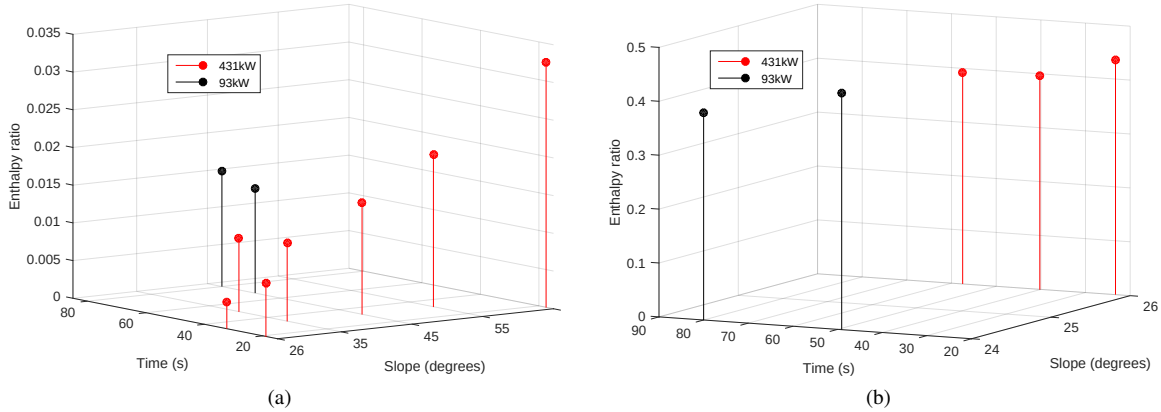

Figure 5. (a) Enthalpy ratio of plumes above and below 1 m high on flat inclined terrains. (b) Enthalpy ratio of plume in and above the narrow 0.55m wide channel running up inclined terrains .

5 Conclusion

Using CFD methods we have produced repeatable and consistent evidence to show channel fires in open terrains produce strong convective winds carrying plumes that attach and follow surfaces of slopes exceeding 26°. For narrow channels such as the rectangular one meter deep by half meter wide example investigated, or those having a narrow floor such as the two meter wide by one meter deep 'V'-shaped example investigated, the plume attachment threshold slope is lowered to 24° or less due to the overlapping influence of significantly steeper compound angles up banks.

For channels above threshold slopes at the scales investigated, at least half the thermal energy released by active fires during a minute or more is retained in the channel and focused on pushing the fire front up through any fuel volume there rather than dissipating skyward. This then is of major significance to firefighters battling wildfires in steep and confined terrains.

Future channel simulations need to investigate the influence of fire source shape and proportion in more channel forms and to quantify buoyancy viscosity relationships associated with fire plume attachment including upper energy intensity limits.

Acknowledgements

This research was funded by the Australian Research Council with computational resources provided under the National Computational Merit Allocation Scheme supported by the Australian Government.

References

ANSYS (2019). *ANSYS CFX-solver modeling guide — release 19.0*. ANSYS Inc.

Cheney, P., J. Gould, and L. McCaw (2001). The dead-man zone - a neglected area of firefighter safety. *Australian Forestry 64*(1), 45–50.

Drysdale, D. D. (1992). Special issue: The king's cross fire. *Fire Saftey Journal 18*, 1–123.

Edgar, R., J. Sharples, and H. Sidhu (2015). Revisiting the Kings Cross underground disaster with implications for modelling wildfire eruption. *21st International Congress on Modelling and Simulation—Modelling and Simulation Society of Australia and New Zealand*, 215–221.

Edgar, R., J. Sharples, and H. Sidhu (2019). The dynamics of channel fire plumes in sloping tunnels. *submitted Fire Safety Journal paper.*.

Schupfer, H. (2001). Fire disaster in the tunnel of the Kitzsteinhorn funicular in Kaprun on 11 Nov. 2000. In *Proceedings of the fourth international conference on safety in road and rail tunnels, held Madrid, Spain, 2-6 April 2001*.

Sharples, J. J., A. M. Gill, and J. W. Dold (2010). The trench effect and eruptive wildfires: lessons from the kings cross underground disaster. In *Proceedings of Australasian Fire Assistance Council*.

Sullivan, A. L., J. Sharples, S. Matthews, and M. P. Plucinski (2014). A downslope fire spread correction factor based on landscape-scale fire behaviour. *Environmental modelling & software 62*, 153–163.

Viegas, D. X., A. Simeoni, G. Xanthopoulos, C. Rossa, L. Ribeiro, L. Pita, D. Stipanicev, A. Zinoviev, R. Weber, J. Dold, et al. (2009). Recent forest fire related accidents in Europe. *Office for Official Publications of the European Communities: Luxembourg*.